Heat Transfer Measurements from a Smooth NACA 0012 Airfoil

Philip E. Poinsatte,* G. James Van Fossen,* and James E. Newton†
NASA Lewis Research Center, Cleveland, Ohio 44135
and
Kenneth J. De Witt‡
University of Toledo, Toledo, Ohio 43606

Local convective heat transfer coefficients were measured from a smooth NACA 0012 airfoil having a chord length of 0.533 m (21 in.). The measurements were made both in flight on the NASA Lewis Twin Otter icing research aircraft and in the NASA Lewis icing research tunnel (IRT). Flight data were taken for the smooth airfoil at Reynolds numbers based on chord in the range 1.24×10^6 to 2.50×10^6 and at various angles of attack up to 4 deg. During these flight tests, the freestream velocity turbulence intensity was found to be very low (<0.1%). Wind tunnel data were acquired in the Reynolds number range 1.20×10^6 to 4.52×10^6 and at angles of attack from −4 to +8 deg. The turbulence intensity in the IRT was 0.5–0.7% with the cloud-generating sprays off. A direct comparison between the results obtained in flight and in the IRT showed that the higher level of turbulence intensity in the IRT had little effect on the heat transfer for the lower Reynolds numbers but caused a moderate increase in heat transfer at the higher Reynolds numbers. Turning on the cloud-generating spray nozzle atomizing air in the IRT did not alter the heat transfer. The present data were compared with leading-edge cylinder and flat plate heat transfer correlations that are often used to estimate airfoil heat transfer in computer codes.

Introduction

THE problem of ice accretion on aircraft has historically drawn considerable attention. The hazards associated with ice formation on wings and engine inlets are well studied and quite apparent. Glaze or rime ice formations on an airfoil add weight, reduce lift, increase drag, and may cause flight control problems. These issues have been discussed by Cebeci,[1] Olsen et al.,[2] Bragg et al.,[3] and Young and Paterson.[4] A further danger arises when pieces of ice fall off a wing or engine inlet and cause damage to parts of the aircraft such as the fan and compressor blades, tail, or rotors. Ice formation on rotary aircraft has drawn much study because of the difficulty of preventing or removing it, as pointed out by Korkan.[5] These problems have once again come into focus for civilian and military aircraft, especially in the application of low-flying missiles and helicopters in regions with cooler climates.

The two general methods used to alleviate the problems of ice accretion are anti-icing and deicing. Anti-icing methods prevent ice from forming, most often by heating the affected area above the water freezing temperature. Deicing methods, on the other hand, remove ice after it begins to grow but before it causes any adverse effects. This is generally accomplished by melting or mechanically cracking the ice and allowing centrifugal or aerodynamic forces to shed it. To apply either of these methods, it is first necessary to attain a good understanding of the icing phenomenon and to be able to predict whether or not ice will grow under specific environmental conditions and for specific locations. Further, ice growth prediction is especially vital in applications in which no ice protection equipment is used. Key to this prediction is the convective heat transfer between the clean surface or the accreted ice and the ambient.

If an aircraft passes through cool air containing supercooled liquid water droplets, an energy balance shows that if the convective and evaporative cooling, as well as the warming of the impinging supercooled droplets to the freezing temperature, can overcome the kinetic and viscous heating and thus remove the latent heat of fusion from the impinging droplets, ice will form on the surface. Hardy,[6] Messinger,[7] and Cansdale and McNaughtan[8] discuss in detail the terms in the energy balance. The dominant heat loss terms in the thermal analysis are convective and evaporative cooling, hence the importance of the local convective heat transfer coefficient h.

Icing facilities and ice accretion modeling codes must simulate accurately the heat transfer occurring in natural icing conditions. Heat transfer is dependent on the freestream turbulence level, and since wind tunnels typically have higher turbulence levels than are found in flight, there may be a problem in using wind tunnels to simulate flight conditions.

One objective of the present study was to determine the differences in local heat transfer from an airfoil between flight and tunnel conditions. A second objective of this work was to obtain much needed airfoil heat transfer data to describe the thermal physics occurring during the icing process and, specifically, to provide accurate airfoil heat transfer data for use in ice growth prediction computer codes. One such code, NASA's LEWICE,[9] currently incorporates an integral boundary-layer subroutine to calculate heat transfer coefficients. Often heat transfer from an airfoil is estimated with cylinder-in-crossflow heat transfer data for the stagnation region and flat plate heat transfer coefficients for the rest of the airfoil surface. The present tests provide actual data for a NACA 0012 airfoil.

Limited data currently exist for heat transfer from an airfoil. NACA studies conducted by Neel et al.[10] and by Gelder and Lewis[11] (1946–1951) compared in-flight heat transfer

Presented in part as Paper 90-0199 at the AIAA 28th Aerospace Sciences Meeting, Reno, NV, Jan. 8–11, 1990; received Sept. 1, 1990; revision received March 31, 1991; accepted for publication April 17, 1991.

*Aerospace Engineer, Internal Fluid Mechanics Division, Heat Transfer Branch.
†Aerospace Engineer, Propulsion Systems Division, Icing and Cryogenic Technology Branch; Deceased.
‡Professor, Department of Chemical Engineering.

from an airfoil, in clear air and during icing conditions, with results from the icing research tunnel (IRT). For the flight data, two separate airfoils, a NACA 0012 and a NACA 65,2-016, were tested at a 0-deg angle of attack, while only the NACA 65,2-016 was subsequently used in the IRT. In the "flat plate" region (i.e., the region away from the stagnation area), the data showed a substantial difference between flight and IRT heat transfer on the forward portion of the airfoil where the boundary layer was laminar. The IRT data were over 30% higher than the flight data. This difference has been attributed to the higher turbulence intensities present in the IRT. This conclusion is also supported by the fact that the flight and IRT data agreed fairly well on the downstream portion of the airfoil where the boundary layer was assumed fully turbulent.

Besides being restricted to a 0-deg angle of attack, two other factors limit the usefulness of the previous data for computer code predictions. First, the data set is incomplete and somewhat inconsistent in the stagnation region, the area where ice growth initiates. Second, data were not taken for a rough surface, which can significantly alter boundary-layer characteristics and thus the local heat transfer. Roughness, the result of early ice growth, may force a laminar boundary layer into transition in the ice formation zone. This behavior was observed in recent experiments performed on a cylinder in crossflow under different turbulence and roughness conditions by Van Fossen et al.[12]

A 1985 study by Pais et al.[13] at the University of Kentucky included the determination of heat transfer coefficients from a smooth NACA 0012 airfoil in a subsonic wind tunnel as well as from a 5 min ice acretion shape. The smooth airfoil measurements were taken at various angles of attack (-8 through $+8$ deg) and for a chord-based Reynolds number range of 7.6×10^5 to 2.0×10^6. The 0-deg angle of attack data generally agreed with the NACA study, and the data showed a larger angle dependence on the suction side as compared with the pressure side. Again, however, more complete roughness data are lacking.

The present study focused on heat transfer measurements on a NACA 0012 airfoil. The NACA 0012 was chosen because it is a symmetric profile that is commonly used in helicopter main rotor and tail rotor applications where it may not be possible to control ice growth by electric heating or pneumatic boots. Local heat transfer coefficients were calculated from measurements taken on the forward 8% chord of a smooth NACA 0012 airfoil with a 0.533 m (21 in.) chord length. Measurements were also taken on the same airfoil with a roughened surface and are presented in an engineering note. Heat transfer measurements were recorded in flight on the NASA Lewis Twin Otter icing research aircraft and in the NASA Lewis IRT. Flight data were collected at various aircraft speeds and various angles of attack up to 4 deg. Data were acquired in the IRT at various tunnel airspeeds, with and without spray nozzle atomizing air, and for various angles of attack from -4 deg (heat flux gauges on the pressure side) to $+8$ deg (heat flux gauges on the suction side). Selected data from the IRT and flight tests will be presented here as Frossling number vs position on the airfoil for various angles of attack. Stagnation region data are compared with Frossling's[14] cylinder-in-crossflow solution, and data further aft on the airfoil are compared with flat plate correlations.[15] Complete results are available in Ref. 16.

Experiment Equipment and Procedure

Apparatus

NACA 0012 Test Airfoil

Heat transfer measurements were made on a NACA 0012 airfoil that was constructed of mahogany and had a chord length of 0.533 m (21 in.) and a span length of 1.8 m (6 ft). The airfoil is shown in Fig. 1. An array of heat transfer gauges was located in a removable section at the center of the span. The gauges were constructed of aluminum and were 6.60 cm (2.60 in.) long in the spanwise direction, 0.476 cm (0.1875 in.) wide in the flow direction, and 0.318 cm (0.125 in.) deep. Each heat flux gauge was equipped with a type E thermocouple and thin foil heater that were connected to individual control circuits that allowed the gauges to be operated in a constant temperature mode. The surface of each gauge was polished to a mirror finish. Figure 2 shows a cross section of the airfoil and

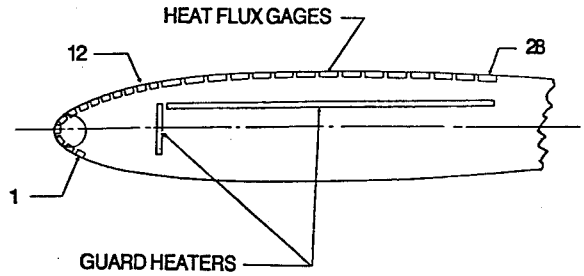

Fig. 2 Cross section of airfoil with heat flux gauges.

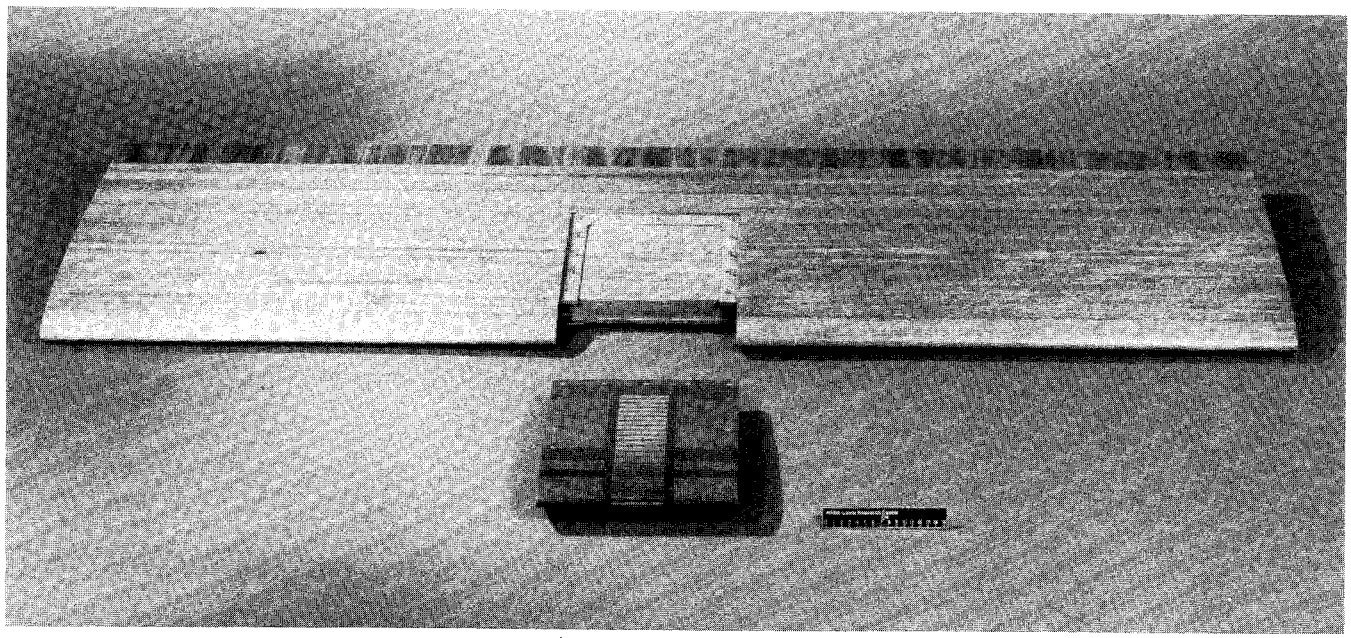

Fig. 1 NACA 0012 test airfoil.

the location of the heat transfer gauges, along with the associated guard heaters. Table 1 lists the dimensionless surface distance (s/c), where c is the chord length, from the geometric stagnation point to the center of each gauge, along with the gauge heat transfer surface area. The airfoil actually contained 28 heat flux gauges, but only 12 of them in the forward region were used in this study. A computerized data acquisition system was employed to record voltage and current input to each gauge as well as gauge temperature. Further details of the model and instrumentation can be found in Ref. 16.

Twin Otter Aircraft

The NACA 0012 airfoil was flown atop the NASA Lewis Twin Otter icing research aircraft. The aircraft with airfoil mounted is shown during a checkout flight in Fig. 3. Details of the twin engine aircraft and parameter measurements are found in Ref. 16. With the NACA 0012 research airfoil mounted vertically on the top of the aircraft, the maximum sustainable speed was around 69 m/s (154 mph) at 1585–2250 m (5200–7400 ft) pressure altitude and a temperature range of 10–21°C (50–70°F). Variance of the test airfoil angle of attack was achieved through yawing the aircraft with a combination of rudder and aileron.

Icing Research Tunnel

The NACA 0012 heat transfer airfoil was also tested in the NASA Lewis icing research tunnel (IRT). The IRT is a closed-loop subsonic refrigerated air tunnel used primarily for icing studies. A plan view of the IRT is shown in Fig. 4. Airflow is induced by a 5000 hp, 7.31 m (24 ft) diam fan, and airspeed in the 1.83 by 2.74 m (6 × 9 ft) test section can be varied from about 9 to 125 m/s (20–280 mph). The air is cooled by passage through a heat exchanger unit that maintained total air temperature around −6.7°C (20°F), plus or minus 0.55°C (1°F). Spray bars located approximately 14.6 m (48 ft) upstream of the test section are used to produce the icing cloud. The spray bars contain a collection of spray nozzles that shoot a combination of pressurized air and water to yield a continuous and uniform cloud of very small supercooled water droplets. The spray bars are also heated with a separate closed steam loop to prevent the nozzles from freezing up. The liquid water content of the tunnel icing cloud can generally range from about 0.2 to 3.0 g/m^3, and the drop diameter can range from about 5 to 40 μm.[17] Typical cloud conditions require the nozzle atomizing spray air to be set at 60 psi and, due to facility constraints, roughly 82°C (180°F). In the present heat transfer tests, ice growth on the airfoil was to be avoided; therefore, when the spray bars were employed, only the 60 psi air was used. No water was passed through the nozzles.

The airfoil was mounted vertically on the turntable in the floor of the test section as shown in Fig. 5. Details of the airfoil mounting and flow parameter measurements are found in Ref. 16.

Table 1 Location and surface area of heat transfer gauges

Gauge	s/c	Surface area, cm^2
1	−0.036	3.145
2	−0.024	3.145
3	−0.012	3.145
4	0.000	3.187
5	0.012	3.145
6	0.024	3.145
7	0.036	3.145
8	0.048	3.145
9	0.060	3.145
10	0.072	3.145
11	0.083	3.145
12	0.095	3.145

Test Procedure

Turbulence Measurements

All turbulence measurements were made with a standard constant temperature hot-wire anemometer operating in an uncalibrated mode.[18] The probe consisted of a single tungsten wire.

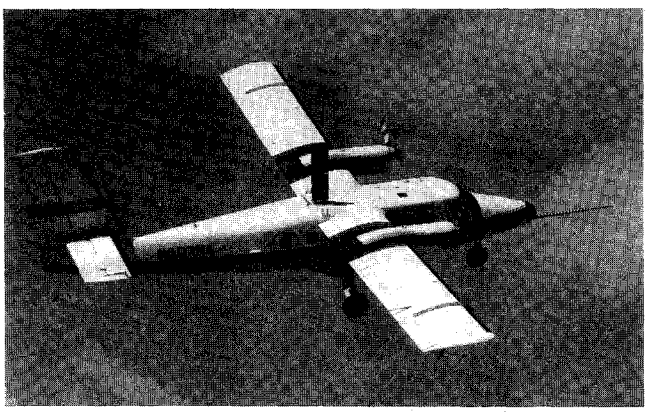

Fig. 3 NASA Lewis icing research aircraft with research airfoil.

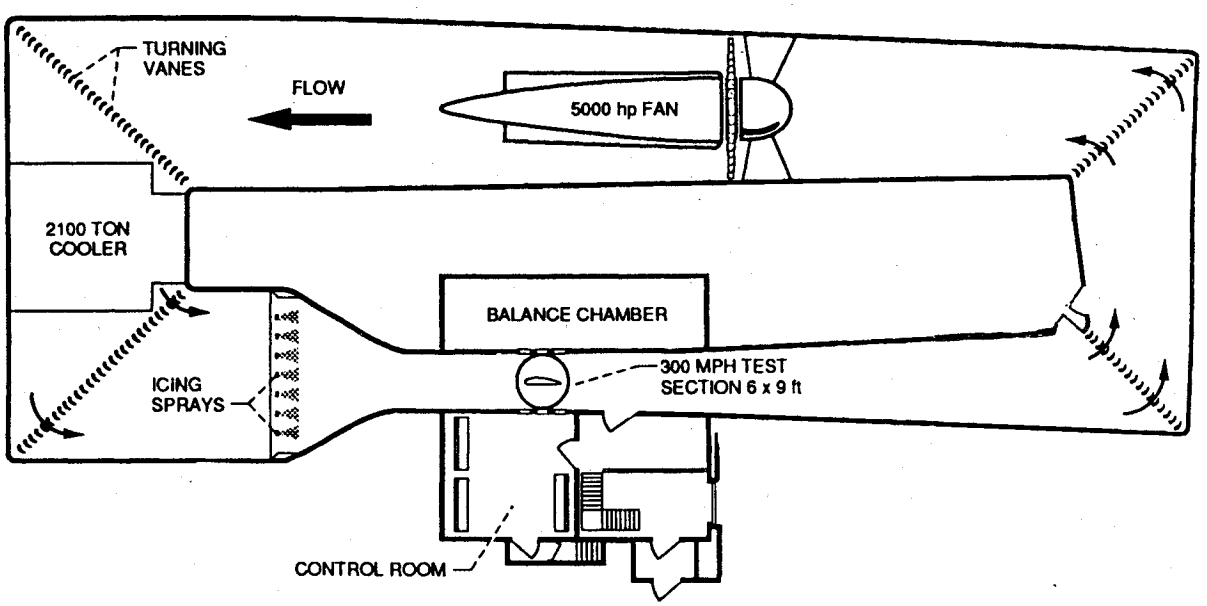

Fig. 4 NASA Lewis icing research tunnel.

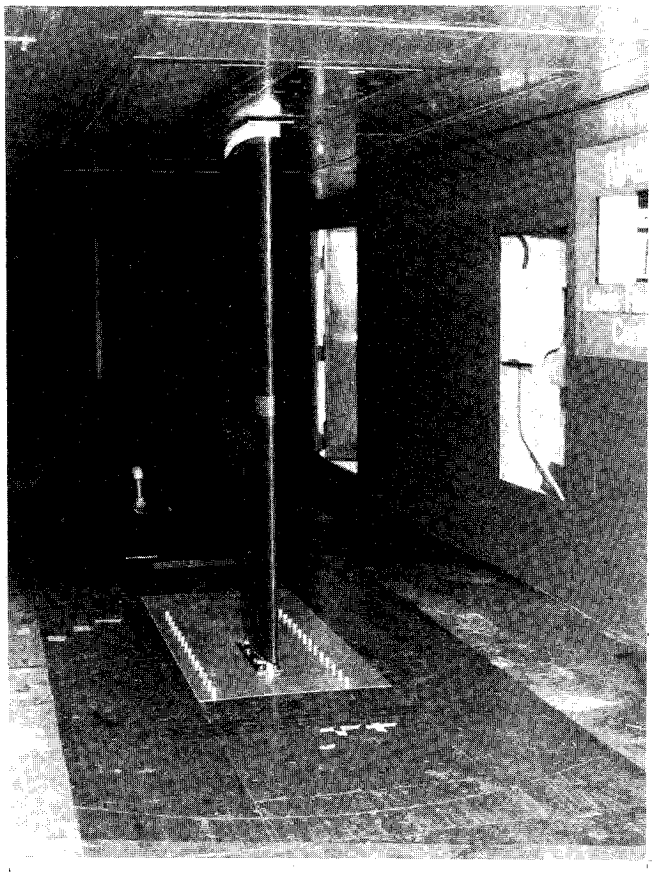

Fig. 5 Test airfoil positioned in the icing research tunnel.

Turbulence measurements were made on two different flights. The first flight was a preliminary test without the test airfoil in place to determine if turbulence from any part of the aircraft structure would interfere with the heat transfer measurements. The probe was mounted about 0.9 m (3 ft) above the fuselage in the same position as the test airfoil heat flux gauges. The second flight took place with the test airfoil in place and the hot wire mounted about 2.8 m (9 ft) forward of the airfoil and slightly offset from the centerline. It was determined from the hot-wire measurements that turbulence generated by the aircraft was not a problem. In both flights, the turbulence intensity was found to be too low to make a meaningful measurement ($< 0.1\%$) for smooth air.

Turbulence measurements were made in the IRT with the same constant temperature hot-wire equipment that was used in the flight tests. The probe was positioned in the center of the tunnel about 0.31 m (1 ft) in front of the gauges on the test airfoil. Turbulence intensities were measured with the cloud-making nozzle atomizing air sprays off and were found to be equal to or less than 0.7% for freestream velocities up to 94 m/s (210 mph). Turbulence measurements with the cloud-making air sprays turned on were found to be difficult to measure with hot-wire equipment because the ambient tunnel air temperature generally averaged 6.7°C (20°F) whereas the spray air temperature had to be maintained near 82°C (180°F) due to facility limitations. Since the hot wire is a heat transfer sensing device, turbulence readings would be affected by this temperature difference and would not measure true turbulent velocity fluctuations.

Flight Heat Transfer Measurements

All heat transfer data acquisition flights were made in darkness to avoid solar radiation on the gauges and the airfoil. Flights were conducted at an altitude that provided smooth atmospheric conditions. Ambient air temperature was generally in the range of 10–21°C (50–70°F).

When steady-state airflow conditions were established at the desired airspeed and angle, the heated aluminum strips were adjusted to a uniform temperature that was typically in the range of 32–41°C (90–105°F). When steady-state thermal conditions were reached, data recording was initiated. About 2 min were required to obtain and record the required 10 scans of all data channels.

Icing Research Tunnel Heat Transfer Measurements

The heat transfer tests done in the IRT were performed in much the same way as the flight tests. After the initial tunnel cooldown, the heat transfer experiments were begun. The tunnel air temperature was around −6.7°C (20°F). The airfoil angle of attack was set by rotating the turntable to the desired position and the tunnel air velocity was varied by adjusting the fan speed. When steady-state tunnel conditions were achieved, the airfoil heaters were adjusted to a uniform temperature, typically in the range of 32–38°C (90–100°F). Again, data recording was initiated after steady-state thermal conditions were obtained. Roughly 2 min were required to obtain and record 10 scans of all data channels. Runs were made with and without the cloud-generating spray air turned on.

Data Reduction

The average heat transfer coefficient from each gauge was obtained from the applied voltage and current and the calculated temperature difference between the gauge and the freestream total temperature. Since only the convective heat transfer was desired, the radiation heat loss had to be subtracted from the total electric power input to each heater. Further, the heater gauges embedded in the airfoil were secured in place and separated from each other by an epoxy resin. Some heat was conducted from the edges of each heater gauge through the epoxy and convected from the surface of the airfoil in the gaps between the gauges and from the unguarded ends of the gauges. These losses were also subtracted from the electric power. Therefore, the local convective heat transfer coefficient h for each aluminum heater gauge was calculated from

$$h = (Q_{ei} - Q_{\text{rad}} - Q_{\text{gap}} - Q_{\text{end}})/[A\,(T_g - T_t)] \qquad (1)$$

where Q_{ei} (voltage x current) is the total electric power input to each heater. The quantity Q_{rad} is the radiation heat loss, which is estimated by

$$Q_{\text{rad}} = \sigma A\,\epsilon\,(T_g^4 - T_t^4) \qquad (2)$$

A value of 0.045 was used for ϵ, the emissivity of polished aluminum, and σ is the Stefan-Boltzmann constant. The quantities Q_{gap} and Q_{end} are the heat lost through the epoxy gaps separating the aluminum gauges and the unguarded ends of the heaters, respectively. These quantities were obtained from an exact solution for heat conduction in a rectangle with appropriate boundary conditions, which is detailed in Ref. 16. In general, Q_{gap} equaled 15% of the total electric power supplied, while Q_{end} and Q_{rad} equaled 4% and 1%, respectively. The remaining quantities are A, the surface area of each aluminum strip; T_g, the measured wall temperature of each gauge; and T_t, the total temperature. For the flight data, T_t was calculated from the measured static temperature T_s and the true airspeed, i.e.,

$$T_t = T_s(1 + M/5) \qquad (3)$$

where M is the Mach number. Typical values for T_t ranged from 10 to 21°C (50–70°F). For the IRT data, T_t was measured with two thermocouples positioned on the leading edge of the airfoil and was typically around −6.7°C (20°F).

The heat transfer data in this analysis are presented as a Frossling number based on chord length that is calculated as

$$Fr = Nu/Re^{0.5} = (hc/k)/(\rho Vc/\mu)^{0.5} \qquad (4)$$

The quantity Nu is the Nusselt number, Re is the Reynolds number, and c is the 0.533 m (21 in.) chord length. The density ρ was calculated from the ideal gas relation for air using the static temperature and pressure at the test airfoil location. The velocity V for flight data was measured with Twin Otter instrumentation and converted to the true test section velocity with the aid of calibrations obtained on previous Twin Otter flights, whereas the velocity for the tunnel data was measured with the IRT pitot static probe. The thermal conductivity k and viscosity μ were obtained as functions of temperature from air data in Ref. 19. These thermal properties were evaluated at the film temperature given by

$$T_f = (T_g + T_t)/2 \tag{5}$$

An uncertainty analysis according to the method of Kline and McClintock[20] was performed on the calculated local heat transfer coefficient and the Frossling number. The uncertainties for each gauge were similar and averaged around 4.5% for h and 5% for Fr. A substantial part of this uncertainty was found to be due to uncertainty in the gap heat loss term because the thermal conductivity of the epoxy gap material was not known exactly and was assumed to be 0.19 W/m K (with a 50% uncertainty), a typical value for epoxy of this nature. This would not be a random error but would tend to bias the data either high or low. However, good general agreement with flat plate data seemed to confirm that the epoxy thermal conductivity value used was correct.

Results and Discussion

In this section selected results of the heat transfer tests conducted in the IRT as well as data obtained during the Twin Otter aircraft flights will be presented. Special emphasis is given to the effect on heat transfer of the different freestream turbulence levels. The turbulence intensity measured with hot-wire equipment during the flight runs was found to be very low (<0.1%). However, in the IRT with the cloud-making sprays off, the turbulence intensity level was found to be 0.62, 0.52, and 0.7% at tunnel air speeds of 31, 63, and 94 m/s (70, 140, and 210 mph), respectively. Previous studies measured the IRT turbulence levels to be around 0.5% with the cloud-making air sprays off and around 2% with spray equipment operating; however, this latter result is somewhat suspect because of the aforementioned concerns regarding the required spray air temperature.

Generally, the IRT data exhibited the same trends as the flight data. Figure 6 shows the Frossling number based on chord as a function of s/c for the smooth airfoil at 0-deg angle of attack at various Reynolds numbers for the flight tests. Figure 7 shows similar conditions for IRT data with and without tunnel spray air. The data plotted in this manner collapse onto a single curve that shows the Nusselt number is proportional to the square root of the Reynolds number. A least squares curve fit[16] of the equation

$$Nu = A\,(Re)^B \tag{6}$$

for the tunnel data showed that the Nusselt number did correlate with the Reynolds number raised to the 0.5 power. The flight Nusselt number data more accurately correlated with the Reynolds number raised to a power of around 0.43. However, a sufficiently good correlation with the square root of the Reynolds number was found to justify presentation of the data as a Frossling number. The solid line on Fig. 7 represents the averaged, smooth-surface, 0-deg angle-of-attack flight data and will be reproduced on subsequent figures for reference. As expected, the Frossling number is greatest at the stagnation point and then trails off smoothly to an average value of around 1.0 at an s/c value of 0.083. The IRT stagnation point average value of 4.56 is only 6% higher than the average stagnation value of 4.30 for the flight data. The correlations developed by Lowery and Vachon[21] predict a stagnation point heat transfer enhancement of 3.5% due to 0.7% freestream turbulence at a Reynolds number of 1.2×10^6 and 5.9% at a Reynolds number of 3.5×10^6. The reason for the "bump" at $s/c = 0.048$ is unknown; there were no obvious rough spots or steps on the surface of the airfoil at this or any other point.

For comparison purposes, representative cases of tunnel and flight data under similar conditions (i.e., same angle of attack and comparable Reynolds numbers) will be presented.

Figure 8 shows the heat transfer results for both spray conditions of the IRT tests as well as for the flight test. These data

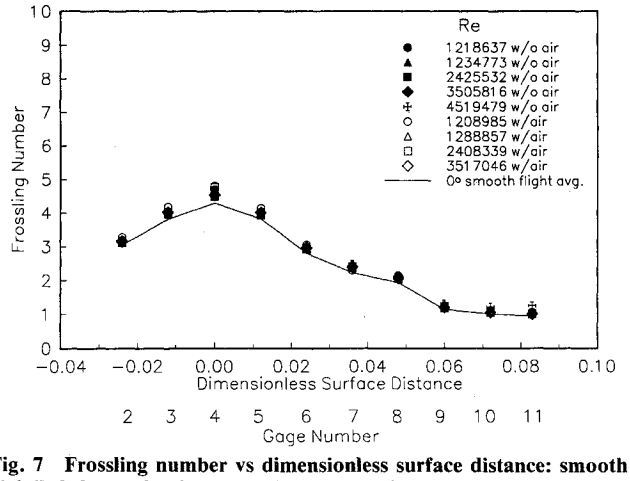

Fig. 7 Frossling number vs dimensionless surface distance: smooth airfoil, 0-deg angle of attack, without and with spray nozzle atomizing air, IRT data.

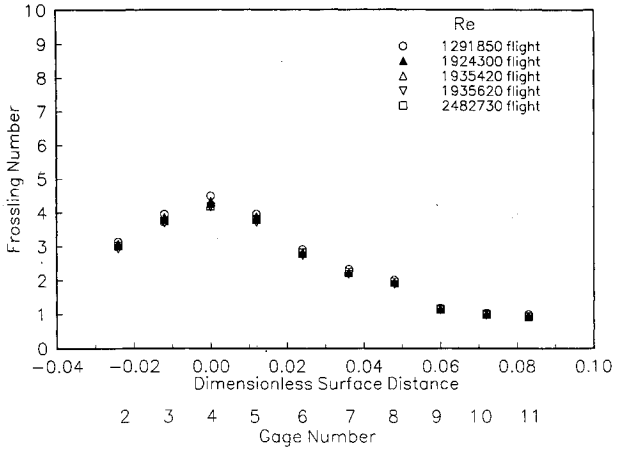

Fig. 6 Frossling number vs dimensionless surface distance: smooth airfoil, 0-deg angle of attack, flight data.

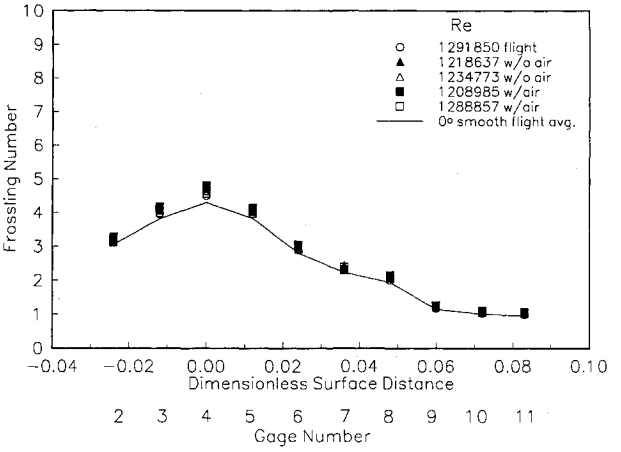

Fig. 8 Frossling number vs dimensionless surface distance: smooth airfoil, 0-deg angle of attack, $Re = 1.2 \times 10^6$, flight and IRT data.

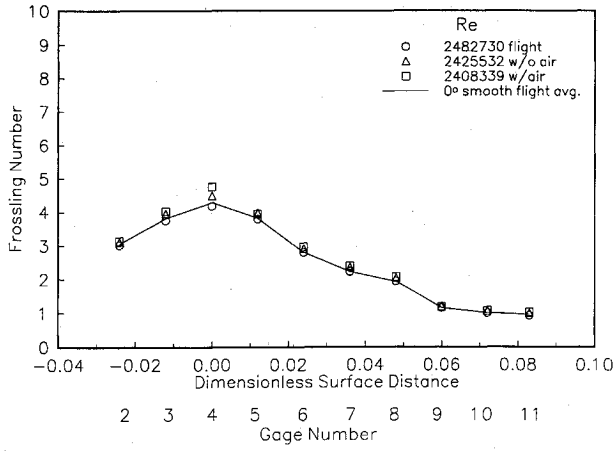

Fig. 9 Frossling number vs dimensionless surface distance: smooth airfoil, 0-deg angle of attack, $Re = 2.4 \times 10^6$, flight and IRT data.

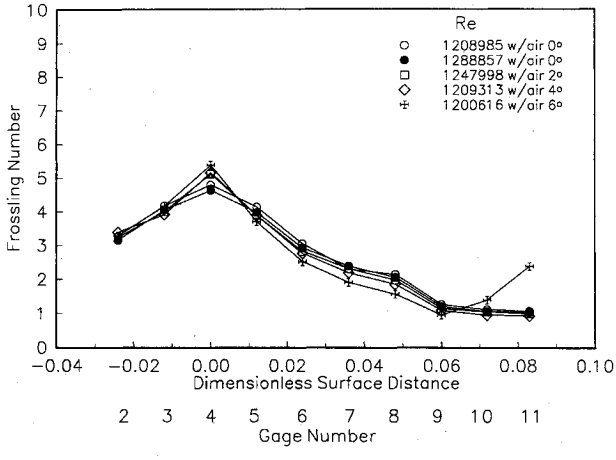

Fig. 10 Frossling number vs dimensionless surface distance: smooth airfoil, $Re = 1.2 \times 10^6$, with spray air, IRT data.

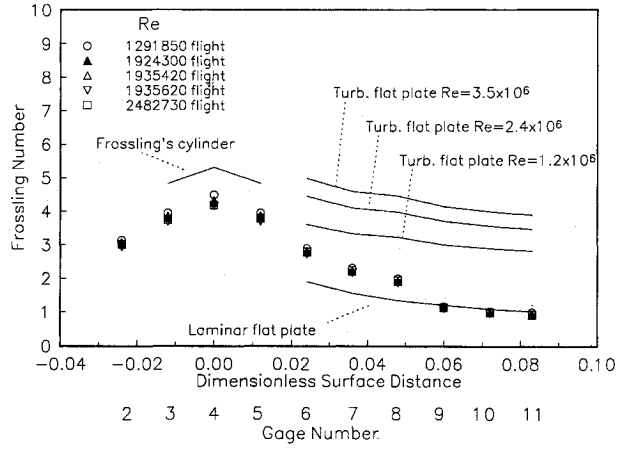

Fig. 11 Frossling number vs dimensionless surface distance: smooth airfoil, 0-deg angle of attack, flight data vs dimensionless correlations for cylinder[14] and flat plate.[15]

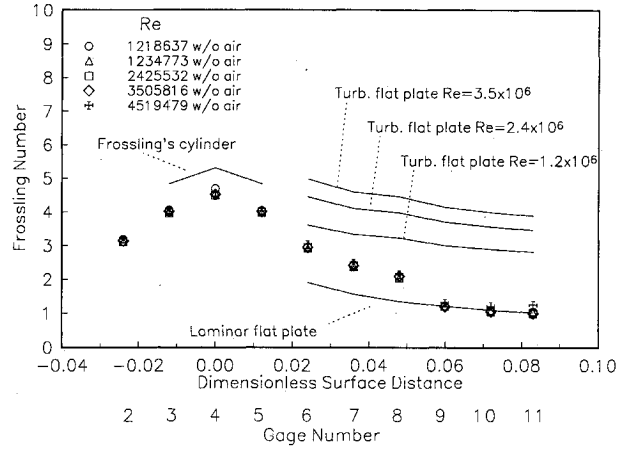

Fig. 12 Frossling number vs dimensionless surface distance: smooth airfoil, 0-deg angle of attack, IRT data (without spray air) vs dimensionless correlations for cylinder[14] and flat plate.[15]

are for the smooth airfoil at a 0-deg angle of attack and a nominal Reynolds number equal to 1.2×10^6. Compared with the flight data, gauges 2–6 show a Frossling number only 2–3% higher for the tunnel cases without spray air and 3–5% higher with spray air. Further aft on the airfoil ($s/c > 0.03$), the Frossling number averages 6% higher than the flight data for both with and without spray air cases. All of these values are within the limits of the calculated experimental uncertainty.

Figure 9 shows similar Frossling number behavior for a nominal Reynolds number of 2.4×10^6. The two tunnel cases, with and without spray air, again agree quite well (within 2%). However, comparing both cases with the flight data shows that the Frossling number tunnel data are roughly 7% higher on gauges 2–6 and 10% higher on gauges greater than 6. The 2- and 4-deg angle-of-attack smooth-airfoil data exhibited similar behavior, showing good general agreement between tunnel and flight data at the lower Reynolds numbers, whereas at the higher Reynolds numbers the Frossling numbers for the tunnel cases were somewhat higher than the flight data.

It seems evident that the small increase in turbulence level has a slight effect on the heat transfer that is magnified with increasing Reynolds number. A consequence of this behavior is seen in the Nusselt vs Reynolds number power law constants. Generally, the exponents on the downstream gauges of the IRT data are slightly higher than the corresponding flight data. Further, and perhaps more importantly, the addition of spray air (recall that in these experiments only spray air and not any spray water was turned on) to the tunnel stream does not affect the heat transfer and thus apparently does not affect the turbulence level. It should be mentioned, however, that it is possible that the spray air does increase the tunnel turbulence but the leading-edge heat transfer is not sensitive to this change.

The general Frossling number dependence on angle of attack is illustrated in Fig. 10 for the smooth airfoil. Figure 10 shows IRT with spray air Frossling number data for the smooth airfoil at a 1.2×10^6 nominal Reynolds number for 0-, 2-, 4-, and 6-deg angles of attack. Data for the suction side of the airfoil are represented by positive s/c values. The stagnation gauge heat transfer generally increases with angle of attack, whereas the first pressure gauge decreases, going from 0 to 2 to 4 deg, then increases from 4 to 6 deg. This behavior can be explained by the movement of the aerodynamic stagnation point; the stagnation region sees an effectively larger leading-edge radius as it moves toward gauge 3 with 2- and 4-deg angles of attack, and this results in a lower heat transfer coefficient. The flow is then accelerated around the leading edge, thus increasing the heat transfer at the geometric stagnation point. Similarly, going to 6 deg moves the aerodynamic stagnation point toward gauge 2, causing an increase in gauge 3 heat transfer. It should also be noted that the power law curve fits showed that as the aerodynamic stagnation point moves closer to the pressure side gauges (gauges 2 and 3), the $Re^{0.5}$ dependence is seen to exist at those gauges, i.e., the Nusselt number at the aerodynamic stagnation point always has an $Re^{0.5}$ dependence. On the suction side, the heat transfer generally decreases with angle. However, at 6 deg, the data illustrate a drastic rise in heat transfer at s/c greater than 0.06, which is most likely due to boundary-layer transition. Data were also acquired at a −4-deg angle of attack that allowed more complete measurement of pressure side heat transfer values. Com-

paring the −4-deg (pressure side) data with the +4-deg (suction side) data showed that for the smooth airfoil the pressure side heat transfer was slightly higher than the suction side.

It is possible to define the Frossling number in terms of the diameter of a cylinder inscribed in the leading edge of the airfoil. This allows comparison of Frossling's[14] analytical solution for heat transfer in the stagnation region of a circular cylinder with the present data. For a NACA 0012 airfoil, the leading edge equivalent diameter is 3.16% of the chord or 0.0169 m (0.664 in.) for the airfoil tested[22] (see Fig. 2). The experimental average Frossling number based on leading-edge equivalent diameter for the smooth airfoil was found to be 0.76 for the flight data and 0.806 for IRT data, roughly 20% and 15% lower, respectively, than the 0.945 value predicted by Frossling's cylinder solution. Frossling's analytical results are often used with an equivalent leading-edge diameter to compute heat transfer in the stagnation region for airfoils and turbine blades. However, it is uncertain as to whether the validity of this method has been proven experimentally.

In computer codes, heat transfer from airfoils is often estimated by using cylinder-in-crossflow heat transfer values in the leading-edge region and flat plate heat transfer values further aft. Figures 11 and 12 show chord-based Frossling number values corresponding to Frossling's[14] analytical cylinder-in-crossflow solution, together with laminar and turbulent flat plate values,[15] on the same graphs as the present 0-deg, smooth-airfoil flight and tunnel data (without spray air), respectively. Both graphs show good agreement with the laminar flat plate correlation at s/c greater than 0.06, the flight data averaging around 8% lower and the tunnel data around 3% higher. However, in the stagnation region, the experimental heat transfer is somewhat lower than that predicted by Frossling. Gauges 2–5 show a 19–21% lower Frossling number for the flight data and 14–17% lower for the tunnel data. In addition, both the flight and the IRT data fall between the laminar and turbulent flat plate values for $0.01 < s/c < 0.06$. It seems, therefore, that the inscribed cylinder method for estimating the heat transfer from the forward portion of a NACA 0012 airfoil does not accurately work; in this case the method substantially overpredicts the measured heat transfer.

Conclusions

Local heat transfer measurements from a smooth NACA 0012 airfoil were successfully obtained in flight and in the NASA Lewis icing research tunnel using the method and apparatus described in this work.

Major conclusions resulting from this study are the following:

1) The smooth airfoil Frossling number data for flight with a measured turbulence intensity of <0.1% and for the IRT with a 0.5–0.7% turbulence intensity showed fairly good agreement at the lower Reynolds number ($Re = 1.2 \times 10^6$). At the higher Reynolds number ($Re = 2.4 \times 10^6$), the IRT data were somewhat higher than the flight data.

2) The IRT is a fairly clean wind tunnel, with a measured turbulence intensity around 0.5–0.7%. The addition of spray air to the tunnel flow did not change the heat transfer, indicating that the turbulence level was not significantly altered by the spray air.

3) Generally, the suction-side heat transfer on the smooth airfoil slowly decreased with angle of attack. However, at 6 deg the downstream heat transfer drastically increased, indicating that some flow transition had occurred. The Nusselt number for the smooth-airfoil cases at the aerodynamic stagnation point always correlated with $Re^{0.5}$.

4) The flight and tunnel smooth airfoil data show good agreement with the laminar flat plate heat transfer values for s/c equal to or greater than 0.06. In the leading-edge region, the measured heat transfer is somewhat lower than that predicted by Frossling's laminar flow cylinder solution: 15% lower in the IRT and 20% lower in flight. Therefore, it would appear that the method of using an inscribed cylinder for approximating the leading-edge heat transfer does not work for the NACA 0012 airfoil.

Acknowledgment

This work was supported under Grant NAG 3-72 by the NASA Lewis Research Center, Cleveland, Ohio.

References

[1]Cebeci, T., "Effects of Environmentally Imposed Roughness on Airfoil Performance," NASA CR-179639, June 1987.

[2]Olsen, W. A., Shaw, R. J., and Newton, J. E., "Ice Shapes and the Resulting Drag Increase for a NACA-0012 Airfoil," NASA TN-83556, Jan. 1984.

[3]Bragg, M. B., Gregorek, G. M., and Shaw, R. J., "Wind Tunnel Investigation of Airfoil Performance Degradation Due to Icing," AIAA Paper 82-0582, Jan. 1982.

[4]Young, A. D., and Paterson, J. H., "Aircraft Excrescence Drag," AGARDograph 264, July 1981.

[5]Korkan, K. D., "Performance Degradation of Propeller-Rotor Systems Due to Rime Ice Accretion," NASA Lewis Research Center Icing Analysis Workshop, Cleveland, OH, Feb. 1983.

[6]Hardy, J. K., "Protection of Aircraft Against Ice," Royal Aircraft Establishment, Rept. S.M.E. 3380, Farnborough, Hampshire, England, UK, July 1946.

[7]Messinger, B. L., "Equilibrium Temperature of Unheated Icing Surface as a Function of Airspeed," *Journal of Aeronautical Sciences,* Vol. 20, No. 1, Jan. 1953, pp. 29–42.

[8]Cansdale, J. T., and McNaughtan, I. I., "Calculation of Surface Temperature and Ice Accretion Rate in a Mixed Water/Ice Crystal Cloud," Royal Aircraft Establishment, TR 77090, Farnborough, Hampshire, England, UK, June 1977.

[9]Ruff, G. A., and Berkowitz, B. M., "Users Manual for the NASA Lewis Ice Accretion Prediction Code (LEWICE)," NASA CR-185129, May 1990.

[10]Neel, C. B., Bergrun, N. R., Jukoff, D., and Schlaff, B. A., "The Calculation of Heat Required for Wind Thermal Ice Prevention in Specified Icing Conditions," NACA TN-1472, Dec. 1947.

[11]Gelder, T. F., and Lewis, J. P., "Comparison of Heat Transfer from Airfoil in Natural and Simulated Icing Conditions," NACA-2480, Sept. 1951.

[12]Van Fossen, G. J., Simoneau, R. J., Olsen, W. A., and Shaw, R. J., "Heat Transfer Distributions Around Nominal Ice Accretion Shapes Formed on a Cylinder in the NASA Lewis Icing Research Tunnel," AIAA Paper 84-0017, Jan. 1984; see also NASA TM-83557, Jan. 1984.

[13]Pais, M. R., Singh, S. N., and Zou, L., "Determination of the Local Heat Transfer Characteristics on Glaze Ice Accretions on a NACA-0012 Airfoil," AIAA Paper 88-0292, Jan. 1988.

[14]Frossling, N., "Evaporation, Heat Transfer, and Velocity in Two-Dimensional and Rotationally Symmetrical Laminar Boundary Layer Flow," NACA TM-1432, Feb. 1958.

[15]Welty, J. R., Wicks, C. E., and Wilson, R. E., *Fundamentals of Momentum, Heat, and Mass Transfer,* Wiley, New York, 1984, p. 370.

[16]Poinsatte, P. E., "Heat Transfer Measurements from a NACA 0012 Airfoil in Flight and in the NASA Lewis Icing Research Tunnel," M.S. Thesis, Univ. of Toledo, Toledo, OH, June 1989; see also NASA CR-4278, March 1990.

[17]Anon., "Icing Research Tunnel," ASME International Historic Landmark Ceremony, NASA B-87-0011, May 1987.

[18]Anon., "Hot Wire and Hot Film Measurements and Applications," Thermal Systems, Inc., Tech. Bulletin No. 4, St. Paul, MN, Jan. 1966.

[19]Hillsenrath, J., Beckett, C. W., Benedict, W. S., Fano, L., and Hobe, H. J., "Tables of Thermal Properties of Gases," National Bureau of Standards Circular 564, Washington, DC, Nov. 1955.

[20]Kline, S. J., and McClintock, F. J., "Describing Uncertainties in Single Sample Experiments," *Mechanical Engineering,* Vol. 75, No. 1, Jan. 1953, pp. 3–8.

[21]Lowery, G. W., and Vachon, R. I., "The Effect of Turbulence on Heat Transfer from Heated Cylinders," *International Journal of Heat and Mass Transfer,* Vol. 18, No. 11, 1975, pp. 1229–1241.

[22]Abott, I. H., von Doenhoff, A. E., and Stivers, L. S., "Summary of Airfoil Data," NACA Rept. 824, March 1945.